Clinical Neurophysiology 130 (2019) 331–340

Contents lists available at ScienceDirect

Clinical Neurophysiology

journal homepage: www.elsevier.com/locate/clinph

Investigating dynamic functional network patterns after propofol-induced loss of consciousness

Yun Zhang [a,1], Chunshu Wang [b,1], Yubo Wang [a], Fei Yan [b], Qiang Wang [b], Liyu Huang [a,*]

[a] School of Life Science and Technology, Xidian University, Xi'an, China
[b] Department of Anesthesiology, The First Affiliated Hospital of Xi'an Jiaotong University, Xi'an, China

ARTICLE INFO

Article history:
Accepted 25 November 2018
Available online 27 December 2018

Keywords:
Anesthesia
Dynamic functional connectivity
Clustering
EEG source imaging

HIGHLIGHTS

- Dynamic brain functional network during anesthesia is supported by 5 metastable network patterns.
- The occurrence of each metastable network pattern is associated with the level of anesthesia.
- An anatomical connectivity supported functional network pattern persists across conscious levels.

ABSTRACT

Objective: We investigated the changes of dynamic brain functional network from awaken state to the anesthesia level suitable for surgery.
Methods: 60-channel EEG data of 22 subjects are acquired at wakefulness, light anesthesia and deep anesthesia. The activity of 68 cortical regions are obtained by using EEG source imaging. Sliding window analysis is employed to obtain a dynamic sequence of brain functional network. K-means clustering algorithm is then employed to identify the common brain functional network patterns.
Results: Five common brain functional network patterns were identified across all conscious levels. The occurrence of each meta-stable network pattern was associated with the level of anesthesia. A transition functional network pattern was found to transfer to the anesthesia dominating or wakefulness dominating network pattern depending on the conscious level. Furthermore, a functional network pattern persisted during both wakefulness and anesthesia is found to be supported by the anatomical connectivity.
Conclusions: Dynamic changes of brain functional network exist in both awaken and anesthesia state.
Significance: These findings suggest that dynamic brain functional network analysis plays a critical role in decoding the mechanism of general anesthesia. The obtained five metastable network patterns may be employed for monitoring the depth of anesthesia.

1. Introduction

General anesthesia is a drug-induced, revisable state of unconsciousness (Brown et al., 2010). On the molecular level, various anesthetic agents bind to their designated targets such as γ-aminobutyric acid (GABA) and N-methyl-D-aspartate (NMDA), which results in an enhanced inhibitory tone (Franks, 2008; Alkire et al., 2008). The change in the inhibitory/excitatory state of the neural cells then disrupts the information transmission and gives rise to the suppression of consciousness (Brown et al., 2011). On the macroscopic scale, brain network analysis revealed that loss of responsiveness to external stimulus was accompanied with the disruption of frontal-to-parietal information transmission (Lee et al., 2011, 2013b). Moreover, reconfigured hub structure and reduced network efficiency were consistently observed during anesthetic-induced loss of responsiveness (Schroter et al., 2012; Lee et al., 2013a; Blain-Moraes et al., 2014; Kim et al., 2016).

Existing investigations of anesthetic induced changes on the brain functional network have extended our knowledge on the mechanism of anesthetic-induced unconsciousness. There are however two issues need to be resolved before these mechanism researches can be utilized in clinical settings. Firstly, using behavior marker as indication of loss of consciousness is problematic (Sanders et al., 2012). It has been demonstrated that the required plasma/effect concentration of anesthetic for inducing unconsciousness during surgery is twice as much as that

* Corresponding author.
E-mail address: huangly@mail.xidian.edu.cn (L. Huang).
[1] Both authors contributed equally to this work.

https://doi.org/10.1016/j.clinph.2018.11.028
1388-2457/

required for inducing loss of response to external stimulus (Ni Mhuircheartaigh et al., 2013). Since the brain functional network may behave differently under higher dose of anesthetics, it is therefore desirable to characterize the brain functional network at the anesthesia level suitable for surgery. Secondly, existing works mostly employed a static approach in which the brain functional network structure was assumed to be the same at the same conscious state, *i.e.* awake or unconsciousness (Lee et al., 2013a; Kim et al., 2016). Yet, recent studies demonstrated that changes of the brain functional connectivity appear to be varying at the time scales from seconds to minutes (Deco et al., 2013). Such non-stationary characteristics of brain functional connectivity was showed to be independent of cognitive process and conscious state (Chang and Glover, 2010; Hutchison et al., 2013). Hence, the brain may still function in a dynamic way even after unconsciousness.

Recently, attempts have been made to investigate the dynamic pattern of brain functional network under anesthesia (Barttfeld et al., 2015; Kafashan et al., 2016). The measured brain activity such as fMRI or EEG was first isolated in time domain by using a sliding window approach. Brain connectivity measure was then estimated on each sliding window to form a dynamic sequence along the temporal domain. Then, the clustering analysis was applied to the obtained dynamic sequence to identify the co-varied functional connectivity pattern across conscious level (Kafashan et al., 2016). However, such method can not reveal the transition behavior of the dynamic brain functional network. To access the dynamic brain functional connectivity on a whole, it is more reasonable to cluster the estimated time-varying brain functional networks across time and conscious level (Allen et al., 2014).

In the present study, we aimed at investigating the dynamic changes of the brain functional network from awaken state to the anesthetized state which is suitable for performing surgery. To do so, 60-channel EEG data were recorded during wakefulness, light anesthesia and deep anesthesia that were defined by the bispectral index (BIS) value. Electrical source images of the EEG (ESI) was obtained to locate the cortical activity (Michel et al., 2001, 2004). Then, time-varying functional connectivity between brain regions was estimated by using sliding-window correlation analysis. K-means clustering was used to identify the common brain functional network patterns. The transition behavior of these reoccurring network patterns at wakefulness, light and deep anesthetized state can reveal how the brain functional network patterns being dynamically affected by the continuous infusion of propofol. Furthermore, we compared the reoccurring functional network patterns across three conscious levels to explore the dynamic brain functional network changes occurred at different conscious level. As numerous studies have shown profound changes in alpha rhythms during anesthesia(Purdon et al., 2013; Vazquez et al., 2014), only alpha band was considered in the present study.

2. Methods

2.1. Participants

The experiment procedure was approved by the ethics review board of the first affiliated hospital of Xi'an Jiaotong University. Experiments were carried out in accordance to the Declaration of Helsinki. Totally, 22 male healthy subjects (35.1 ± 5.7 years of age) participated in this study. All the subjects were fully informed and the written consent form was obtained prior to the experiment. All subjects are drug-free, allergy-friendly to propofol, and have no history of neurological or psychiatric conditions. Each participant fasted for over 8 h and had no pre-medication before the experiment.

2.2. Propofol anesthesia

All the experiments were performed by two experienced anesthesiologists. During the experiment, adequate oxygen was delivered via a face mask. Vital signs including heart rate, blood pressure and oxygen saturation level (SpO_2) were closely monitored by using intra-operative monitors (Philips MP50, Boeblingen, Germany). The anesthesia depth was tracked by using the bispectral index monitor (Covidien, Mansfield, MA, USA).

Propofol (Fresenius Kabi, Graz, Austria) was served as the sole anesthetic in the experiment. Propofol was administered via a target-controlled infusion system based on the Marsh pharmacokinetic model (Injectomat TIVA Agilia, Fresenius Kabi Gmbh, Graz, Austria) (Marsh et al., 1991). The initial target plasma concentration of propofol was set at 2.0 μg/ml. Prior to the administration of propofol, the subjects were asked to keep relaxed and wakeful for 2 min. Subjects were instructed to keep their eyes closed throughout the experiment.

We targeted at two anesthesia endpoints, *i.e.* light anesthesia and deep anesthesia, by using the BIS value. The light and deep anesthesia was defined as the BIS value falls into the range of 60 ± 5 and 40 ± 5, respectively (Liu et al., 1997; Struys et al., 1998). The plasma concentration of propofol was carefully controlled with a step-size of 0.2 μg/ml until achieving the predefined anesthesia endpoints. At each anesthesia level, the BIS value was kept stable within the pre-defined range for at least 2 min. After completing the data acquisition at deep anesthesia level, the reverse protocol was initiated by setting the plasma concentration of propofol to 0 μg/ml, and the subjects were pushed into the anesthesia recovery room to wait for the full recovery.

2.3. EEG acquisition and analysis

2.3.1. Pre-processing

60-channels EEG data was recorded using Synamps 2/RT system (NeuroScan, Singen, Germany). The EEG signal was sampled at 1 kHz. Electrode impedance was kept below 5 kΩ throughout the experiment. All the channels were referenced to the left and right mastoids. The EEG data was first band-pass filtered in the frequency of alpha band (8–12 Hz). Artifacts were removed by visual inspection. The artifact-free EEG signals were re-referenced to the common average reference. A block diagram of EEG signal processing and analysis was shown in Fig. 1.

2.3.2. EEG source imaging analysis

60-s long EEG data was extracted from the pre-processed EEG at each conscious level, *i.e.* the wakefulness, light anesthesia and deep anesthesia. Source reconstruction was performed to obtain the cortical activity with additional benefit of mitigating the effect of volume conduction (Michel et al., 2004). To do so, a reference head model based on a default anatomy derived from the ICBM152 template was firstly generated by using the OpenMEEG boundary element method (Gramfort et al., 2010; Mazziotta et al., 2001). Then, the cortically distributed current density value at 15002 voxels were estimated using the standardized low-resolution brain electromagnetic tomography (sLORETA) algorithm (Pascual-Marqui, 2002). Furthermore, these voxels were segmented into 68 regions-of-interest (ROIs) based on the Desikan-Killiany brain atlas (Desikan et al., 2006). Activity of each ROI was obtained by averaging the current source density of all voxels within that region. All source localization analyses were performed by using Brainstorm (Tadel et al., 2011).

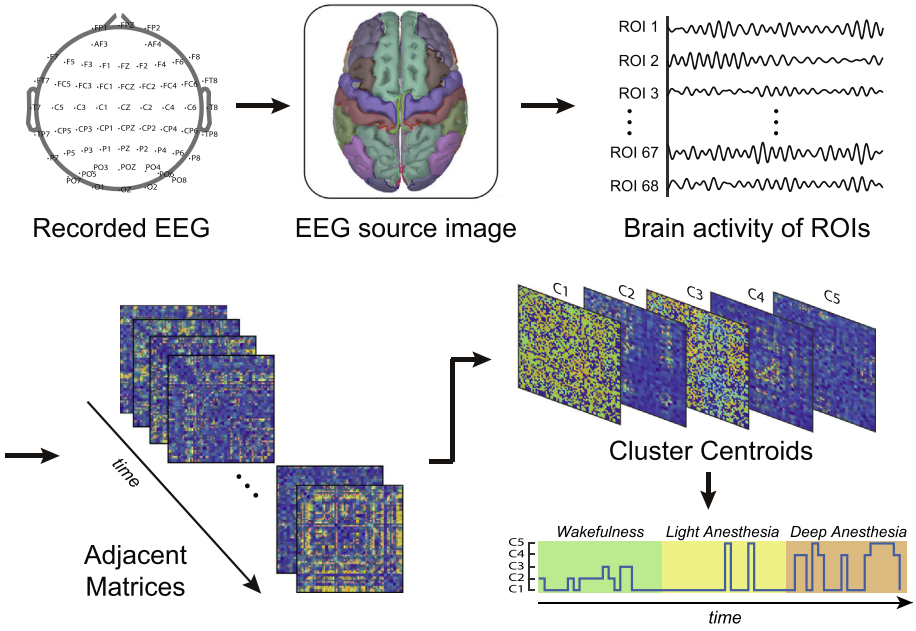

Fig. 1. Schematic diagram of data processing.

2.4. Dynamical functional connectivity analysis

2.4.1. Estimation of functional connectivity

The obtained cortical activity of each ROI was segmented into 1-s window with fifty percent overlap, which results in 119 data segments for one conscious level per subject. The adjacent matrix was estimated using the data from each data segmentation, hence it formed a dynamic sequence of brain functional activity across all three conscious levels. Totally, 357 adjacent matrices were obtained for each subject of all conscious levels. Here, we used the weight phase lag index (wPLI) to measure the connectivity strength between a pair of brain regions (Vinck et al., 2011; Lau et al., 2012). The wPLI is defined as

$$\mathrm{wPLI}_{n_i,n_j,\tau} = \left| \left\langle \frac{\left|\sin(\triangle\Phi_{n_i,n_j,\tau})\right|}{\sin(\triangle\Phi_{n_i,n_j,\tau})} \right\rangle \right| \tag{1}$$

where $\triangle\Phi_{n_i,n_j,\tau} = \Phi_{n_i,\tau} - \Phi_{n_j,\tau}$ represents a vector of phase differences between brain region i and region j at τ-th time window. The phase of information of each brain region $\Phi_{n,\tau}$ was obtained by utilizing Hilbert transform, and it was defined as

$$\Phi_{n,\tau} = \arctan\left(\frac{\tilde{x}(t)}{x(t)}\right) \tag{2}$$

where the $x(t)$ and $\tilde{x}(t)$ represents the real signal and its corresponding Hilbert transform, respectively.

To prevent false connections, the surrogate data based method was employed to obtain the genuine connections (Müller et al., 2008). To do so, 20 surrogate data sets were generated for each time window, in which the power spectra was kept same to the original data, but with randomly assigned phases. A connection was deemed genuine, if its wPLI value deviated from the distribution of the 20 wPLI values obtained from the surrogate data sets. Nonparametric Wilcoxon signed-rank test was performed to evaluate the deviation (H0 [null hypothesis]: the 20 corresponding wPLI values came from the surrogate data sets have symmetric distribution with the wPLI value in the original adjacent matrix) (Lee et al., 2013a). Only genuine connections were retained for further analysis.

2.4.2. Clustering analysis

In our analysis, we obtained 357 adjacent matrices for each subject across all three conscious levels. We polled adjacent matrices from all subjects over all conscious levels to estimate the common brain functional network patterns. Totally, 7854 (357 time windows × 22 subjects) adjacent matrices were obtained. The k-means clustering algorithm based on L_1 distance (Manhattan distance) was employed to access the reoccurring functional network patterns. To remove the redundancy in the obtained brain connectivity estimations, we adopted L1-norm regularized least squares regression (LASSO) to select the most relevant features from the obtained adjacent matrix (Tibshirani, 1996). Finally, 1412 features were identified by using the LASSO regression and were used for the clustering analysis. The number of clusters (k) was determined by the elbow criterion. The clustering algorithm was repeated 500 times with randomly initialized cluster centroids to ensure the validity of the clustering results. Then, each adjacent matrix was assigned to an identified cluster with the closest distance among all cluster centroids.

To quantify the probability that each identified functional network pattern reoccurred at different conscious level, we computed the probability of occurrence of cluster Ci as

$$p_{s,g,Ci} = \frac{\sum_{\tau=1}^{N}(\delta(I_{s,g,\tau} - Ci))}{N}, \delta(x) = \begin{cases} 1 & x = 0 \\ 0 & x = other \end{cases} \tag{3}$$

where $N = 119$ is the number of time windows of the sth subject at gth conscious level. $I_{s,g,\tau}$ represents the cluster index of the τth time window. Hence, $p_{s,g,Ci}$ is a percentage value quantifying the proportion of the identified cluster Ci at a given conscious level.

The transition behavior among the identified common functional network patterns was investigated to explore the temporal dynamic properties of the brain functional network. For each subject and each conscious level, the obtained adjacent matrices were assigned to the identified cluster centroids. Hence, the cluster indexes of the adjacent matrices constituted a dynamic sequence in the temporal domain.

We considered the identified clusters formed a finite state space with maximumly k possible states, denoted as $\{C1, C2, \ldots, Ck\}$. At any given time window, the obtained adjacent matrix will be

assigned to only one state among all identified states. We also assumed that the dynamic sequence of states followed a first-order Markov chain (Balduzzi and Tononi, 2008). Formally, let $X_t \in \{C1, C2, \ldots, Ck\}$ denote the dynamic sequence of states at *t-th* time window. Then, the transition behavior of brain functional network can be investigated by estimating the transition matrix $T_{ij} = P(X_{t+1} = Cj | X_t = Ci)$, with i and j represents the index of state at two consecutive time windows, an illustration of Markov chain with three states was provided in Fig. 2. The transition behavior of a conscious level was obtained by averaging the transition matrices over all subjects. The stationary distribution was estimated to further depict the state distribution if a conscious level could be maintained infinitely. The stationary distribution π of a Markov chain quantifies the proportion of time a state occupies the chain despite the starting state. It satisfies $\pi = \pi T$, and often approximated as the eigenvector corresponds to the unit eigenvalue of T, with T being the transition matrix of Markov chain.

2.5. Statistical analysis

One-way repeated measures ANOVA with a Greenhouse-Geisser correction and a post hoc analysis with Bonferroni correction was employed to compare the probability of occurrence of a identified common brain functional network pattern across three conscious levels (wakefulness, light anesthesia and deep anesthesia). Results are deemed statistically significant when P-value is below 0.05.

Existing studies reported that anesthetic altered the connectivity both within- and between- resting-state networks (RSNs) (Liang et al., 2015; Hashmi et al., 2017). Hence, we assigned each ROI to a RSN based on specific RSN maps (Hashmi et al., 2017), and then compared the differences of the identified common brain functional networks across three conscious levels to explore the dynamic changes of RSNs during propofol infusion. The 68 ROIs used in this study were divided into four RSNs, including the sensory network (SN), the language/memory network (L/MN), the attention/executive network (A/EN) and the default mode network (DMN). The detail parcellation scheme was shown in Table 1. To ensure that only the strongest connections were used in the statistical analysis, the genuine adjacent matrices were thresholded by persevering the top 10% of strongest connections (Tagliazucchi et al., 2012). Then, the adjacent matrix was compressed into a 4×4 connectivity matrix with each node represents an RSN. The weight of each edge in the 4×4 connectivity matrix was the number of top 10% connections between each pair of RSNs. The diagonal element was the number of top 10% connections contained within an RSN. Since we have assigned each adjacent matrix to a cluster, the obtained 4×4 matrices then inherited the cluster index from its corresponding adjacent matrix. Then, we compared

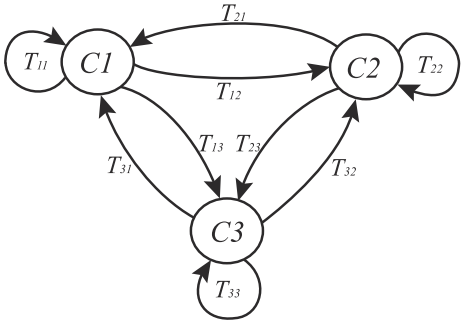

Fig. 2. Schematic of transition behavior between clusters. In the present study, there are totally k possible clusters ($C1, C2, \ldots, Ck$). We just showed 3 clusters here for illustration. T_{ij} represents the transition probability between the clusters Ci and Cj.

Table 1
Resting-state networks, anatomic brain regions.

Networks	Regions
Sensory network	Cuneus
	Fusiform gyrus
	Insula
	Lateral occipital cortex
	Paracentral gyrus
	Pericalcarine cortex
	Postcentral gyrus
	Precentral gyrus
	Precuneus cortex
	Transverse temporal
Language/memory network	Bankssts
	Entorhinal
	Inferior temporal gyrus
	Lingual gyrus
	Middle temporal
	Parahippocampal gyrus
	Superior temporal gyrus
	Temporal pole
Attention/executive network	Caudal middle frontal gyrus
	Frontal pole
	Pars opercularis
	Pars orbitalis
	Pars triangularis
	Rostral middle frontal gyrus
	Superior frontal gyrus
	Superior parietal
	Supramarginal gyrus
Default mode network	Caudal anterior cingulate
	Inferior parietal
	isthmus cingulate
	lateral orbitofrontal
	medial orbitofrontal
	Posterior cingulate
	Rostral anterior cingulate

Each brain region contain two parts, the left and right hemispheres.

the weight of each edge in the generated 4×4 matrices between each pair of clusters by employing two sample t-test. Totally 10 two statistical tests were conducted for each pair of clusters. Hence, Bonferroni correction was applied to mitigate the effect of multiple comparisons, which increased the threshold for statistical significance to $P < 0.05/10 = 0.005$.

3. Results

3.1. Dynamic functional network patterns

Using k-means clustering analysis, we identified 5 clusters that presents across all three conscious levels. Each cluster can be considered as a common brain functional network pattern. We denoted the five clusters as C1, C2, C3, C4 and C5. The probability of occurrence of each cluster at three conscious levels, *i.e.* the wakefulness, light anesthesia and deep anesthesia, were provided in Table 2. The probability of occurrence of clusters were compared across three conscious levels to recognize the dominating pattern at each conscious level. As shown in Fig. 3 and Table 3, we observed that the cluster C1 had the highest probability of occurrence at all three conscious levels (wakefulness: 1555, 59.4%; light anesthesia: 1817, 69.4%; deep anesthesia: 1291, 49.3%). The clusters C2 had higher probability of occurrence at wakefulness (wakefulness: 606, 23.2%), while clusters C4 (light anesthesia: 324, 12.4%; deep anesthesia: 735, 28.1%) and C5 (light anesthesia: 361, 13.8%; deep anesthesia: 358, 13.7%) had higher probability of occurrence at anesthetized state. The high probability of occurrence of cluster C2 at wakefulness indicated that the cluster C2 was the dominating functional network pattern at wakefulness. The high probability of

Table 2
Probability of occurrence of each cluster (C1 to C5) at wakefulness, light anesthesia and deep anesthesia.

Cluster	Probability			Statistics
	Wakefulness	Light anesthesia	Deep anesthesia	
C1	0.5940 ± 0.2016	0.6940 ± 0.1473	0.4931 ± 0.1411	$F(1.883,39.534)=11.672$, $P<0.001$
C2	0.2315 ± 0.1590	0.0294 ± 0.0255	0.0359 ± 0.0252	$F(1.058,22.211)=36.124$, $P<0.001$
C3	0.0714 ± 0.0851	0.0149 ± 0.0340	0.0531 ± 0.0389	$F(1.463,30.721)=8.963$, $P=0.002$
C4	0.0122 ± 0.0175	0.1241 ± 0.1199	0.2807 ± 0.1294	$F(1.844,38.715)=43.019$, $P<0.001$
C5	0.0909 ± 0.0451	0.1375 ± 0.0463	0.1371 ± 0.0464	$F(1.846,38.776)=7.264$, $P=0.003$

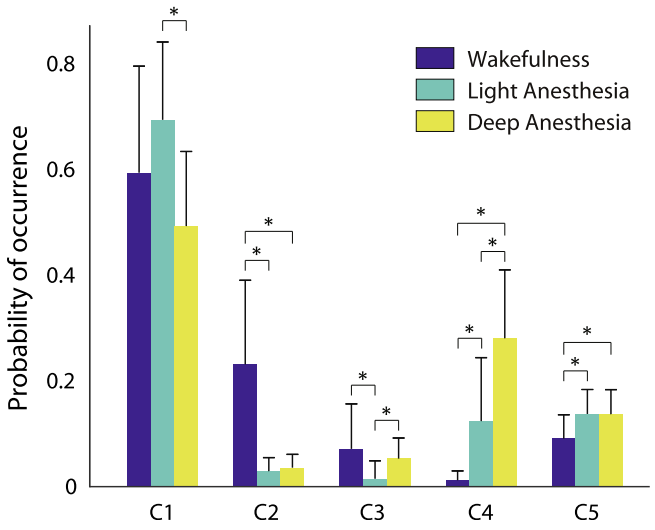

Fig. 3. Probability of occurrence of clusters. The probability of occurrence of each cluster (C1 to C5) at wakefulness, light anesthesia and deep anesthesia. Here * indicates a statistical significant results ($P < 0.05$).

occurrence of clusters C4 and C5 at anesthetized state indicated that the clusters C4 and C5 were the dominating functional network patterns at anesthetized state. Moreover, we found that the probability of occurrence of cluster C4 was varied with the conscious level.

3.2. Transition behavior among functional network patterns

As shown in Fig. 4, values in the transition matrix represent the probability of transforming from one cluster to another. We observed that values in the first column of the transition matrices were high at all three conscious levels, which indicated that cluster C1 had a high probability of maintaining stable and being transformed from other clusters. We also observed that cluster C1 mostly transformed to C2 at wakefulness, whereas it transformed to cluster C4 and C5 at light and deep anesthesia respectively.

At wakefulness, the cluster C2 showed a higher probability of receiving transitions from the clusters C1, C3, C4 and C5. It can be seen that the cluster C2 mostly transformed to the cluster C1 at wakefulness, and to the clusters C1 and C4 during both light anesthesia and deep anesthesia. The cluster C3 had high probability of keeping itself stable during both wakefulness and anesthesia. Cluster C3 mostly transformed to the cluster C2 at wakefulness, and to the cluster C4 during anesthesia. The cluster C4 mostly transformed to the clusters C1 and C2 during wakefulness. While during anesthesia, it had high probability of keeping itself stable. The clusters C5 had high probability of keeping itself stable during both wakefulness and anesthesia, and it constantly had a high probability of transforming to the cluster C1. Moreover, the cluster

Table 3
Comparison of the probability of occurrence of each cluster (C1 to C5) across wakefulness, light anesthesia and deep anesthesia. Values presented here are P values and 95% confidence interval for differences. P < 0.05 were marked in bold.

Cluster	C1	C2	C3	C4	C5
Wakefulness VS *Light anesthesia*	P = 0.073, −0.207–0.007	**P = 0.000, 0.114–0.290**	**P = 0.002, 0.019–0.094**	**P = 0.001, −0.178 to −0.046**	**P = 0.006, −0.081 to −0.012**
Wakefulness VS *Deep anesthesia*	P = 0.119, −0.019 to 0.221	**P = 0.000, 0.113–0.278**	P = 0.832, −0.024–0.061	**P = 0.000, −0.344 to −0.193**	**P = 0.026, −0.088 to −0.005**
Light anesthesia VS *Deep anesthesia*	**P = 0.000, 0.105–0.297**	P = 1.000, −0.024–0.011	**P = 0.001, −0.061 to −0.015**	**P = 0.000, −0.241 to −0.072**	P = 1.000, −0.033–0.034

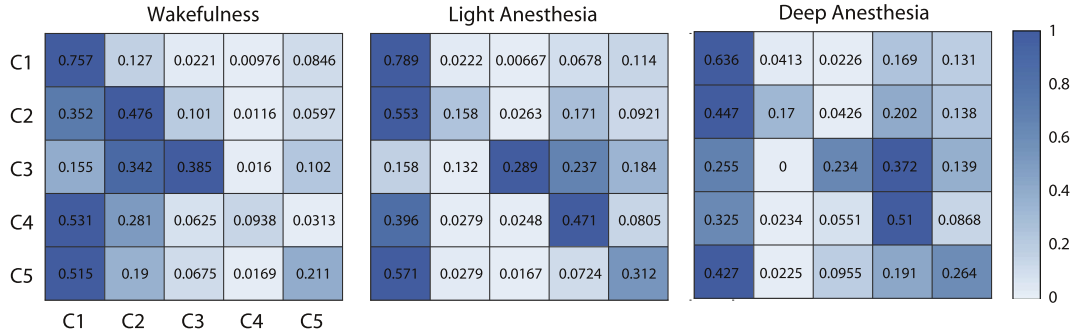

Fig. 4. Transition behavior between clusters. The cluster transition matrices, averaged over subjects at wakefulness, light anesthesia and deep anesthesia. High values was color-mapped in deep color. (For interpretation of the references to colour in this figure legend, the reader is referred to the web version of this article.)

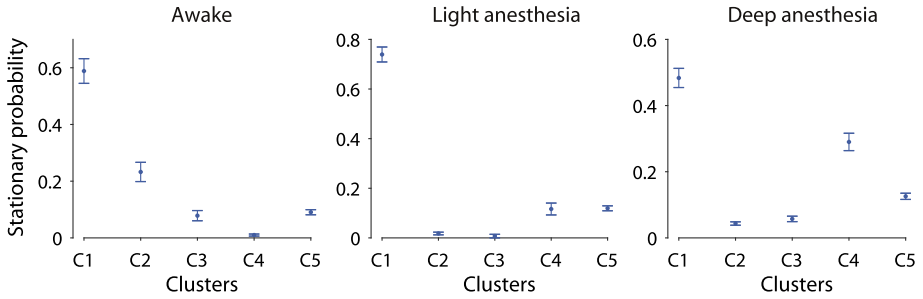

Fig. 5. Stationary distribution π. The stationary probability vectors of the average transition matrix at wakefulness, light anesthesia and deep anesthesia. Error bars indicate the nonparametric 95% confidence intervals (CIs) obtained from 1000 bootstrap resamples of the average transition matrix (resampling subjects).

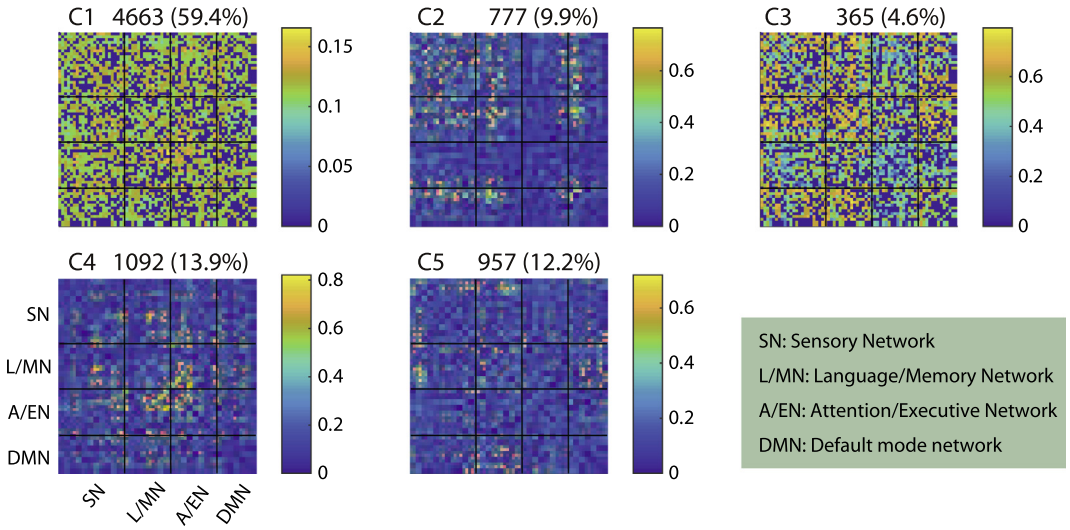

Fig. 6. Clustering results for $k = 5$. Each cluster (C1 to C5) is summarized by its centroid, the total number and percentage of occurrences is listed above each centroid.

C4 and C5 had a higher probability of receiving transitions from the other clusters during anesthesia, especially from the cluster C3.

The stationary distribution (π) obtained for each conscious level was shown in Fig. 5. The high value in π represents that the corresponding cluster was most likely to be found in the long run. We found that the cluster C1 consistently had high values across three conscious levels. The stationary probability of the clusters C2 and C3 was reduced during anesthesia, while the stationary probability of the cluster C4 was increased and it positively related with the depth of anesthesia. The cluster C5 had a higher stationary probability at light anesthesia than at wakefulness, and then it kept stable at deep anesthesia.

3.3. Differences in functional network patterns

The centroid of each identified cluster was shown in Fig. 6. It is clearly that connectivity strength differs among all cluster centroids. To further illustrate the difference in connectivity strength among all clusters, the mean of wPLI values in each adjacent matrix was computed. Then, two sample t test was employed to quantify the difference between each pair of clusters. The results indicated that the cluster C1 had a statistically significant lower ($P < 0.05$) mean functional network connectivity strength than other clusters. The cluster C3 had the largest mean functional network connectivity strength as compared to other clusters. The results were shown in Table 4.

By examining the probability of occurrence of each cluster across three conscious levels, we found that the cluster C2 was the dominating functional network pattern at wakefulness. Therefore, we compared the number of the strongest connections within- and between-RSNsbetween the cluster C2 and the clusters C4 and C5, and between the cluster C3 and the clusters C2 and C4 to identify the changes of the functional network patterns during propofol-induced anesthesia. Since the cluster C4 and C5 showed difference in probability of occurrence and stationary probability during anesthesia, similar comparison was also conductedbetween the cluster C4 and C5.

As shown in Fig. 7 and Table 5, when compared to the cluster C2, the clusters including C3, C4 and C5 presented with more strong connections within A/EN and between A/EN and other RSNs (SN, L/MN and DMN), the clusters C3 and C5 also showed more strong connections within DMN. On the other hand, the cluster

Table 4
Comparison of the mean functional network connectivity strength between each pair of clusters (C1 to C5).

	P value	T value	95% CI
C1 VS C2	< 0.001	−66.1247	−0.0961 to −0.0906
C1 VS C3	< 0.001	−113.0606	−0.2284 to −0.2207
C1 VS C4	< 0.001	−71.9028	−0.0923 to −0.0874
C1 VS C5	< 0.001	−57.8569	−0.0762 to −0.0712
C2 VS C3	< 0.001	−43.8741	−0.1370 to −0.1253
C2 VS C4	0.0986	1.6524	−0.0007–0.0076
C2 VS C5	< 0.001	9.6911	0.0157–0.0237
C3 VS C4	< 0.001	47.0361	0.1290–0.1403
C3 VS C5	< 0.001	55.8062	0.1455–0.1561
C4 VS C5	< 0.001	8.4901	0.0124–0.0199

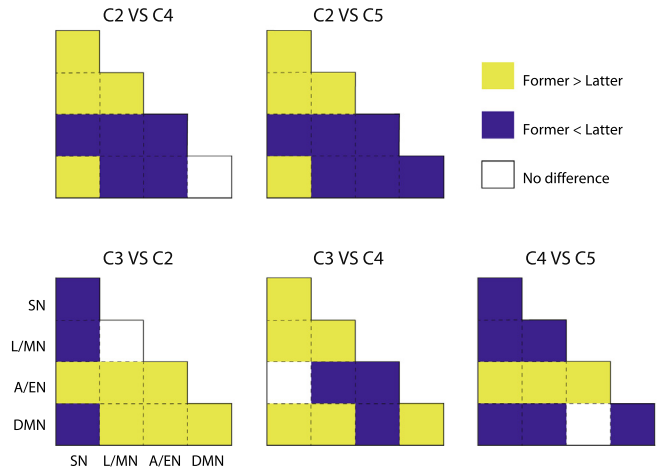

Fig. 7. Differences between clusters. The significant differences of the number of the strongest functional connectivity within and between RSNs. Here $P < 0.005$ is considered to be significant.

C2 showed more strong connections within SN and between SN and L/MN and DMN than that in the clusters C3, C4 and C5, it also had more strong connections within L/MN than the cluster C4 and C5 had. When compared to the cluster C4, the clusters C3 showed less strong connections within A/EN and between A/EN and L/MN and DMN, while it showed more strong connections within- and between-SN, L/MN and DMN. Similar to the cluster C3, the cluster C5 had less strong connections within A/EN and between A/EN and SN and L/MN than the cluster C4 had, and there were more strong connections within- and between-SN, L/MN and DMN in the cluster C5.

3.4. Similarity between anatomical network and functional network patterns

Animal study has shown that brain functional connectivity pattern with a low connectivity strength was closely tied to the anatomical connectivity (Barttfeld et al., 2015). The identified common functional network patterns in this work also presented with large difference in mean strength on the functional network connectivity. Hence, the similarity between the anatomical connectivity and the functional network patterns was estimated to investigate the relationship between the identified common functional network patterns and anatomical network. The anatomical connectivity was obtained from Hagmann et al. (2008). The similarity score was estimated by measuring the correlation between the vectorized structural connectivity matrix (4356×1) and the vectorized centroid of each cluster by using linear regression analysis. As shown in Fig. 8, the cluster C1 had the highest similarity scores 0.1185 ($P < 0.001$) while the cluster C4 had the lowest similarity score 0.0042 ($P > 0.05$), and the similarity scores of the clusters C2, C3, C5 were 0.0239 ($P > 0.05$), 0.0558 ($P < 0.001$), 0.0144 ($P > 0.05$), respectively.

4. Discussion

In the present study, the dynamic changes of brain functional network during propofol-induced anesthesia was investigated. Applying k-means clustering to the obtained dynamic sequence of brain functional networks, five common brain functional

Table 5
Comparison of the strongest functional connectivity within- and between-RSNs. Values presented here are P values, T values and the corresponding 95% confidence interval for differences.

	C2 VS C4	C2 VS C5	C3 VS C2	C3 VS C4	C4 VS C5
Within-SN	$P < 0.001$ T = 30.8841 13.78–15.34	$P < 0.001$ T = 20.8221 10.06–11.79	$P < 0.001$ T = −12.3694 −5.49 to −4.11	$P < 0.001$ T = 8.1816 3.78–5.68	$P < 0.001$ T = −11.4420 −9.63 to −7.36
Within-L/MN	$P < 0.001$ T = 10.6403 6.17 to 8.43	$P < 0.001$ T = 4.2808 2.13–4.79	$P > 0.1$ T = −1.0629 −2.67–0.57	$P < 0.001$ T = 7.5517 4.99–7.77	$P < 0.001$ T = −6.2624 −4.81 to −2.81
Within-A/EN	$P < 0.001$ T = −31.0463 −21.11 to −18.98	$P < 0.001$ T = −20.7790 −12.99 to −11.08	$P < 0.001$ T = 8.6396 4.57–6.72	$P < 0.001$ T = −14.4232 −13.85 to −11.01	$P < 0.001$ T = 15.6012 8.40–10.38
Within-DMN	P = 0.0278 T = 1.9157 0.14–1.90	$P < 0.001$ T = −3.1124 −3.07 to −0.95	$P < 0.001$ T = 3.9070 1.77–4.34	$P < 0.001$ T = 5.5718 2.85–5.23	$P < 0.001$ T = −6.5166 −4.34 to −2.59
L.MN-SN	$P < 0.001$ T = 19.9010 7.81–9.28	$P < 0.001$ T = 13.8597 5.90–7.49	$P < 0.001$ T = −3.9922 −3.65 to −1.52	$P < 0.001$ T = 8.7708 4.11–6.00	$P < 0.001$ T = −5.6357 −2.73 to −1.50
A/EN-SN	$P < 0.001$ T = −9.9466 −3.88 to −2.78	$P < 0.001$ T = −7.1428 −3.21 to −2.01	$P < 0.001$ T = 5.5254 1.87–3.46	$P > 0.1$ T = −0.3380 −0.84–0.55	$P < 0.001$ T = 3.6451 0.56–1.49
A/EN-L/MN	$P < 0.001$ T = −29.1950 −14.08 to −12.58	$P < 0.001$ T = −14.9937 −6.95 to −5.58	$P < 0.001$ T = 9.8964 4.55–6.36	$P < 0.001$ T = −11.1102 −7.91 to −5.87	$P < 0.001$ T = 19.1880 7.19–8.54
DMN-SN	$P < 0.001$ T = 26.3080 8.79–9.96	$P < 0.001$ T = 20.6089 7.44–8.74	$P < 0.001$ T = −3.9883 −3.07 to −1.28	$P < 0.001$ T = 13.2104 5.36–6.89	$P < 0.001$ T = −7.5197 −2.84 to −1.82
DMN-L/MN	$P < 0.001$ T = −7.6880 −4.45 to −2.88	$P < 0.001$ T = −9.8855 −5.90 to −4.21	$P < 0.001$ T = 9.0838 4.61–6.65	P = 0.0037 T = 2.6785 0.65–2.74	$P < 0.001$ T = −3.3445 −2.24 to −0.76
DMN-A/EN	$P < 0.001$ T = −21.1077 −9.10 to −7.79	$P < 0.001$ T = −19.4680 −9.00 to −7.60	$P < 0.001$ T = 8.2575 3.34–5.00	$P < 0.001$ T = −6.4561 −4.36 to −2.59	P = 0.0109 T = 2.2952 0.25–1.51

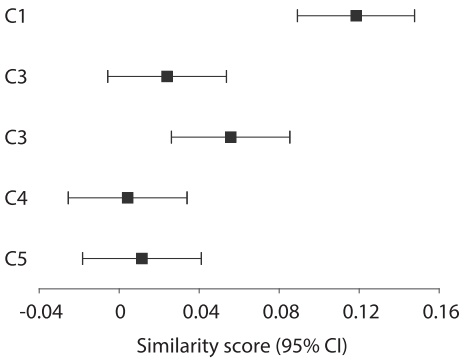

Fig. 8. Similarity score. The similarity between structural connectivity and cluster centroid. The horizontal error bars indicate the 95% CIs.

network patterns emerged. Each functional network pattern had a different probability of occurrence across conscious levels including wakefulness, light and deep anesthesia. The cluster C1 showed high probability of occurrence at all conscious levels, which indicates that the cluster C1 persisted during wakefulness and anesthesia. The dominating functional network pattern at wakefulness was the cluster C2, whereas Clusters C4 and C5 were the dominating brain functional network pattern at anesthetized state.

The cluster C3 was found to be an transition functional network pattern, as it had high probability of transforming to the cluster C2 at wakefulness, and to the cluster C4 during anesthesia. When compared to the cluster C2, the cluster C3 shared similar characteristic with the anesthesia-dominating pattern, *i.e.* there were more strong connections within the A/EN and DMN and between the A/EN and other RSNs. As compared to the anesthesia-dominating functional network pattern, it showed similar characteristics of cluster C2. Hence, the cluster C3 is thought to be an intermediate state between wakefulness and anesthetized states.

Previous animal study using fMRI has shown that the brain functional network with the weakest connectivity strength and high occurrence across conscious levels was probably supported by the anatomical connectivity (Barttfeld et al., 2015). The obtained cluster C1 had the smallest functional connectivity strength among all identified clusters, and it had the highest similarity to the anatomical connectivity. Therefore, the cluster C1 might be the functional network pattern which mediated by the underlying structure of anatomical connectivity. We also found that the cluster C1 constantly had a high probability of occurrence and a high stationary probability during the transition from wakefulness to anesthesia. We could therefore infer that during anesthesia, the functional network pattern which supported by the inherent anatomical connectivity was not affected, and this might also explain why the subjects can maintain physiologically stable during anesthesia, and why anesthetic-induced unconsciousness is reversible, whereas the vegetative state is not (Brown et al., 2010).

Our results revealed that the anesthesia-dominating pattern C4 and C5 had a disrupted brain functional network pattern as compared to the wakefulness-dominating functional network pattern C2 (Boveroux et al., 2010; Liang et al., 2015). The strong cross-RSNs interactions which existed in wakefulness were attenuated under anesthesia, and these altered interactions were mainly located within- and between-SN and L/MN. It has been suggested that the consciousness fundamentally relies on the interactions between brain functional networks which integrate information (Tononi, 2012). Therefore, the disrupted information transfer within- and between-RSNs play a crucial role in propofol-induced unconsciousness.

The generation of a sensory experience or an internal mental activity requires various dynamically interacted brain networks (Crick and Koch, 2003). The dynamic interactions between within- and between-SN and L/MN are the neural basis for supporting the functions such as memory and execution (Crick and Koch, 2003; Dehaene and Changeux, 2011; Hipp et al., 2012). Therefore, the anesthetic-induced amnesia and akinesia might be caused by the disruption of brain functional connectivity between SN and L/MN.

Opposite to the disrupted functional connectivity, we found that the brain presented with strong interactions within DMN and between DMN and A/EN during anesthesia. Previous animal studies suggested that there still exist coherent spontaneous fluctuations among the brain regions which belong to the DMN (Vincent et al., 2007; Lu et al., 2012; Rilling et al., 2007). Since the anesthesia weakened the strong interactions between SN, L/MN and A/EN, we could infer that the strong interactions should mainly located within DMN and between DMN and other RSNs during propofol-induced anesthesia. Furthermore, our findings are similar to the previous works showing hyper-connectivity between the DMN and other brain networks in patients with disorders of consciousness (Di Perri et al., 2013). Such hyper-connectivity may represent dysregulation of a functional loop related to interactions with the external environment and may cause loss of consciousness (Di Perri et al., 2013).

We also found that there were more strong connections between A/EN and the other RSNs during anesthesia, which was one of the notable features of the cluster C4. The probability of occurrence of cluster C4 was found to be positivity correlated with the depth of anesthesia. General anesthesia reduces the fronto-parietal feedback connectivity while preserves the feedforward connectivity (Lee et al., 2009b,a; Ku et al., 2011; Lee et al., 2013b). Such brain network structure may result in a stronger automatic and bottom-up information transfer of external stimulus to anterior brain regions (Uhrig et al., 2016). Our results could partly support this hypothesis. Due to the functional connectivity computed in the present work was unidirectional connectivity, more evidence using directed network is needed in future studies.

Existing depth-of-anesthesia monitoring devices heavily rely on the EEG activity measured from the forehead region. The derived index for anesthesia depth is often obtained by sophisticated and mostly patented algorithms that operate in the frequency domain (Fahy and Chau, 2018). However, the anesthetic agents such as ketamine, nitrous oxide and xenon show distinct EEG spectral patterns due to their difference in the molecular targets (Barttfeld et al., 2015). Therefore, it poses great limitation on the application of current depth-of-anesthesia monitor device. On the other hand, using a network neuroscience approach, the frontal-parietal breakdown and the disrupted efficiency of brain functional networks have been constantly observed on anesthetics with different molecular targets (Lee et al., 2013b; Hashmi et al., 2017). Hence, features obtained from brain functional network analysis are a promising solution for devising an agent-invariant depth-of-anesthesia monitoring system.

Investigating the dynamic changes induced by anesthetics pave the way for realizing such agent-invariant depth-of-anesthesia monitoring system. Our results revealed that brain functional network patterns co-varied with the conscious level. Hence, the anesthesia depth could be inferred by carefully examining the percentage of each brain functional network pattern. However, more works are required before it can be utilized in the clinical settings. Firstly, the relationship between the occurrence of the obtained functional network pattern and a clinical relevant scale such as the observer's assessment of alertness/sedation scale (OAAS) is desired to accurately estimate the conscious level. Moreover, the number of electrodes required for constructing brain

functional network complicates the setup of the system. How to reduce the number of electrodes while keeping the performance in check also requires further investigation.

5. Conclusion

In conclusion, dynamic changes of brain functional network exists in both awaken and anesthesia state. We found that the functional network pattern which was supported by the fundamental anatomical structure of the brain was preserved during anesthesia. There existed an transition functional network pattern during the transition from wakefulness to anesthesia. We also found that the functional network patterns with disrupted connections within- and between-SN, L/MN were exhibited under anesthesia. These findings suggest that dynamic brain functional network analysis plays a critical role in decoding the mechanism of general anesthesia. The obtained five metastable network patterns may be employed for monitoring the depth of anesthesia.

Conflict of interest statement

The authors declare that the research was conducted in the absence of any commercial or financial relationships that could be construed as a potential conflict of interest.

Acknowledgments

This work was financially supported by the National Natural Science Foundation of China under Grant Nos. 81671778, 31271063, 81701787 and U1401255.

References

Alkire MT, Hudetz AG, Tononi G. Consciousness and anesthesia. Science 2008;322:876–80. https://doi.org/10.1126/science.1149213.

Allen EA, Damaraju E, Plis SM, Erhardt EB, Eichele T, Calhoun VD. Tracking whole-brain connectivity dynamics in the resting state. Cereb Cortex 2014;24:663–76. https://doi.org/10.1093/cercor/bhs352.

Balduzzi D, Tononi G. Integrated information in discrete dynamical systems: motivation and theoretical framework. PLoS Comput Biol 2008;4:e1000091. https://doi.org/10.1371/journal.pcbi.1000091.

Barttfeld P, Uhrig L, Sitt JD, Sigman M, Jarraya B, Dehaene S. Signature of consciousness in the dynamics of resting-state brain activity. Proc Natl Acad Sci 2015;112:887–92. https://doi.org/10.1073/pnas.1418031112.

Blain-Moraes S, Lee U, Ku S, Noh G, Mashour GA. Electroencephalographic effects of ketamine on power, cross-frequency coupling, and connectivity in the alpha bandwidth. Front Syst Neurosci 2014;8:1–9. https://doi.org/10.3389/fnsys.2014.00114.

Boveroux P, Vanhaudenhuyse A, Bruno MA, Noirhomme Q, Lauwick S, Luxen A, et al. Breakdown of within- and between-network resting state functional magnetic resonance imaging connectivity during propofol-induced loss of consciousness. Anesthesiology 2010;113:1038–53. https://doi.org/10.1097/ALN.0b013e3181f697f5.

Brown EN, Lydic R, Schiff ND. General anesthesia, sleep, and coma. N Engl J Med 2010;363:2638–50.

Brown EN, Purdon PL, Van Dort CJ. General anesthesia and altered states of arousal: a systems neuroscience analysis. Annu Rev Neurosci 2011;34:601–28. https://doi.org/10.1146/annurev-neuro-060909-153200.

Chang C, Glover GH. Time-frequency dynamics of resting-state brain connectivity measured with fMRI. Neuroimage 2010;50:81–98. https://doi.org/10.1016/j.neuroimage.2009.12.011.

Crick F, Koch C. A framework for consciousness. Nat Neurosci 2003;6:119–26. https://doi.org/10.1038/nn0203-119.

Deco G, Jirsa VK, McIntosh AR. Resting brains never rest: computational insights into potential cognitive architectures. Trends Neurosci 2013;36:268–74. https://doi.org/10.1016/j.tins.2013.03.001.

Dehaene S, Changeux JP. Experimental and theoretical approaches to conscious processing. Neuron 2011;70:200–27. https://doi.org/10.1016/j.neuron.2011.03.018.

Desikan RS, Ségonne F, Fischl B, Quinn BT, Dickerson BC, Blacker D, et al. An automated labeling system for subdividing the human cerebral cortex on MRI scans into gyral based regions of interest. Neuroimage 2006;31:968–80. https://doi.org/10.1016/j.neuroimage.2006.01.021.

Di Perri C, Bastianello S, Bartsch AJ, Pistarini C, Maggioni G, Magrassi L, et al. Limbic hyperconnectivity in the vegetative state. Neurology 2013;81:1417–24. https://doi.org/10.1212/WNL.0b013e3182a43b78.

Fahy BG, Chau DF. The technology of processed electroencephalogram monitoring devices for assessment of depth of anesthesia. Anesth Analg 2018;126:111–7. https://doi.org/10.1213/ANE.0000000000002331.

Franks NP. General anaesthesia: from molecular targets to neuronal pathways of sleep and arousal. Nat Rev Neurosci 2008;9:370–86. https://doi.org/10.1038/nrn2372.

Gramfort A, Papadopoulo T, Olivi E, Clerc M. OpenMEEG: opensource software for quasistatic bioelectromagnetics. Biomed Eng Online 2010;9:45. https://doi.org/10.1186/1475-925X-9-45.

Hagmann P, Cammoun L, Gigandet X, Meuli R, Honey CJ, Wedeen VJ, et al. Mapping the structural core of human cerebral cortex. PLoS Biol 2008;6:e159. https://doi.org/10.1371/journal.pbio.0060159.

Hashmi JA, Loggia ML, Khan S, Gao L, Kim J, Napadow V, et al. Dexmedetomidine disrupts the local and global efficiencies of large-scale brain networks. Anesthesiology 2017;126:419–30. https://doi.org/10.1097/ALN.0000000000001509.

Hipp JF, Hawellek DJ, Corbetta M, Siegel M, Engel AK. Large-scale cortical correlation structure of spontaneous oscillatory activity. Nat Neurosci 2012;15:884–90. https://doi.org/10.1038/nn.3101.

Hutchison RM, Womelsdorf T, Gati JS, Everling S, Menon RS. Resting-state networks show dynamic functional connectivity in awake humans and anesthetized macaques. Hum Brain Mapp 2013;34:2154–77. https://doi.org/10.1002/hbm.22058.

Kafashan M, Ching S, Palanca BJA. Sevoflurane alters spatiotemporal functional connectivity motifs that link resting-state networks during wakefulness. Front Neural Circ 2016;10:1–6. https://doi.org/10.3389/fncir.2016.00107.

Kim M, Mashour GA, Moraes SB, Vanini G, Tarnal V, Janke E, et al. Functional and topological conditions for explosive synchronization develop in human brain networks with the onset of anesthetic-induced unconsciousness. Front Comput Neurosci 2016;10. https://doi.org/10.3389/fncom.2016.00001.

Ku SW, Lee U, Noh GJ, Jun IG, Mashour GA. Preferential inhibition of frontal-to-parietal feedback connectivity is a neurophysiologic correlate of general anesthesia in surgical patients. PLoS One 2011;6:e25155. https://doi.org/10.1371/journal.pone.0025155.

Lau TM, Gwin JT, McDowell KG, Ferris DP. Weighted phase lag index stability as an artifact resistant measure to detect cognitive EEG activity during locomotion. J Neuroeng Rehabil 2012;9:47. https://doi.org/10.1186/1743-0003-9-47.

Lee H, Mashour GA, Noh GJ, Kim S, Lee U. Reconfiguration of network hub structure after propofol-induced unconsciousness. Anesthesiology 2013a;119:1347–59. https://doi.org/10.1097/ALN.0b013e3182a8ec8c.

Lee U, Kim S, Noh GJ, Choi BM, Hwang E, Mashour GA. The directionality and functional organization of frontoparietal connectivity during consciousness and anesthesia in humans. Conscious Cogn 2009a;18:1069–78. https://doi.org/10.1016/j.concog.2009.04.004.

Lee U, Ku S, Noh G, Baek S, Choi B, Mashour Ga. Disruption of frontal-CParietal communication by ketamine, propofol, and sevoflurane. Anesthesiology 2013b;118:1264–75. https://doi.org/10.1097/ALN.0b013e31829103f5.

Lee U, Mashour GA, Kim S, Noh GJ, Choi BM. Propofol induction reduces the capacity for neural information integration: Implications for the mechanism of consciousness and general anesthesia. Conscious Cogn 2009b;18:56–64. https://doi.org/10.1016/j.concog.2008.10.005.

Lee U, Müller M, Noh GJ, Choi B, Mashour GA. Dissociable network properties of anesthetic state transitions. Anesthesiology 2011;114:872–81. https://doi.org/10.1097/ALN.0b013e31821102c9.

Liang P, Zhang H, Xu Y, Jia W, Zang Y, Li K. Disruption of cortical integration during midazolam-induced light sedation. Hum Brain Mapp 2015;36:4247–61. https://doi.org/10.1002/hbm.22914.

Liu J, Singh H, White PF. Electroencephalographic bispectral index correlates with intraoperative recall and depth of propofol-induced sedation. Anesth Analg 1997;84:185–9. https://doi.org/10.1213/00000539-199701000-00033.

Lu H, Zou Q, Gu H, Raichle ME, Stein EA, Yang Y. Rat brains also have a default mode network. Proc Natl Acad Sci 2012;109:3979–84. https://doi.org/10.1073/pnas.1200506109.

Marsh B, White M, Morton N, Kenny G. Pharmacokinetic model driven infusion of propofol in children. Br J Anaesth 1991;67:41–8. https://doi.org/10.1093/bja/67.1.41.

Mazziotta J, Toga A, Evans A, Fox P, Lancaster J, Zilles K, et al. A probabilistic atlas and reference system for the human brain: International Consortium for Brain Mapping (ICBM). Philos Trans R Soc B Biol Sci 2001;356:1293–322. https://doi.org/10.1098/rstb.2001.0915.

Michel CM, Murray MM, Lantz G, Gonzalez S, Spinelli L, Grave de Peralta R. EEG source imaging. Clin Neurophysiol 2004;115:2195–222. https://doi.org/10.1016/j.clinph.2004.06.001.

Michel CM, Thut G, Morand S, Khateb A, Pegna AJ, Grave de Peralta R, et al. Electric source imaging of human brain functions. Brain Res Rev 2001;36:108–18. https://doi.org/10.1016/S0165-0173(01)00086-8.

Müller M, Baier G, Rummel C, Schindler K. Estimating the strength of genuine and random correlations in non-stationary multivariate time series. EPL (Europhys Lett) 2008;84:10009. https://doi.org/10.1209/0295-5075/84/10009.

Ni Mhuircheartaigh R, Warnaby C, Rogers R, Jbabdi S, Tracey I. Slow-wave activity saturation and thalamocortical isolation during propofol anesthesia in humans. Sci Transl Med 2013;5:208ra148. https://doi.org/10.1126/scitranslmed.3006007.

Pascual-Marqui RD. Standardized low-resolution brain electromagnetic tomography (sLORETA): technical details. Methods Find Exp Clin Pharmacol 2002;24 Suppl D:5–12.

Purdon PL, Pierce ET, Mukamel EA, Prerau MJ, Walsh JL, Wong KFK, et al. Electroencephalogram signatures of loss and recovery of consciousness from propofol. Proc Natl Acad Sci 2013;110:E1142–51. https://doi.org/10.1073/pnas.1221180110.

Rilling JK, Barks SK, Parr LA, Preuss TM, Faber TL, Pagnoni G, et al. A comparison of resting-state brain activity in humans and chimpanzees. Proc Natl Acad Sci 2007;104:17146–51. https://doi.org/10.1073/pnas.0705132104.

Sanders RD, Tononi G, Laureys S, Sleigh JW. Unresponsiveness ≠ unconsciousness. Anesthesiology 2012;116:946–59. https://doi.org/10.1097/ALN.0b013e318249d0a7.

Schroter MS, Spoormaker VI, Schorer A, Wohlschlager A, Czisch M, Kochs EF, et al. Spatiotemporal reconfiguration of large-scale brain functional networks during propofol-induced loss of consciousness. J Neurosci 2012;32:12832–40. https://doi.org/10.1523/JNEUROSCI.6046-11.2012.

Struys M, Versichelen L, Byttebier G, Mortier E, Moerman A, Rolly G. Clinical usefulness of the bispectral index for titrating propofol target effect-site concentration. Anaesthesia 1998;53:4–12. https://doi.org/10.1111/j.1365-2044.1998.00279.x.

Tadel F, Baillet S, Mosher JC, Pantazis D, Leahy RM. Brainstorm: a user-friendly application for MEG/EEG analysis. Comput Intell Neurosci 2011;2011:1–13. https://doi.org/10.1155/2011/879716.

Tagliazucchi E, von Wegner F, Morzelewski A, Brodbeck V, Laufs H. Dynamic BOLD functional connectivity in humans and its electrophysiological correlates. Front Hum Neurosci 2012;6:339. https://doi.org/10.3389/fnhum.2012.00339.

Tibshirani R. Regression selection and shrinkage via the lasso. J R Stat Soc Ser B 1996;58:267–88. https://doi.org/10.2307/2346178.

Tononi G. Integrated information theory of consciousness: an updated account. Arch Ital Biol 2012;150:293–329. https://doi.org/10.4449/aib.v149i5.1388.

Uhrig L, Janssen D, Dehaene S, Jarraya B. Cerebral responses to local and global auditory novelty under general anesthesia. Neuroimage 2016;141:326–40. https://doi.org/10.1016/j.neuroimage.2016.08.004.

Vazquez R, Prerau MJ, Ph D, Harrell PG, Hartnack KE, Rhee J, et al. A comparison of propofol- and dexmedetomidine- induced electroencephalogram dynamics using spectral and coherence analysis. Anesthesiology 2014;121:978–89. https://doi.org/10.1097/ALN.0000000000000419.

Vincent JL, Patel GH, Fox MD, Snyder AZ, Baker JT, Van Essen DC, et al. Intrinsic functional architecture in the anaesthetized monkey brain. Nature 2007;447:83–6. https://doi.org/10.1038/nature05758.

Vinck M, Oostenveld R, Van Wingerden M, Battaglia F, Pennartz CM. An improved index of phase-synchronization for electrophysiological data in the presence of volume-conduction, noise and sample-size bias. Neuroimage 2011;55:1548–65. https://doi.org/10.1016/j.neuroimage.2011.01.055.